



Dalton
Transactions

**Advances in magnetic films of epsilon-iron oxide toward
next-generation high-density recording media**

Journal:	<i>Dalton Transactions</i>
Manuscript ID	DT-FRO-10-2020-003460.R1
Article Type:	Frontier
Date Submitted by the Author:	22-Nov-2020
Complete List of Authors:	Tokoro, Hiroko; University of Tsukuba; The University of Tokyo, Department of Chemistry, School of Science Namai, Asuka; The University of Tokyo School of Science, Department of Chemistry Ohkoshi, Shin-ichi; The University of Tokyo, Department of Chemistry, School of Science

SCHOLARONE™
Manuscripts

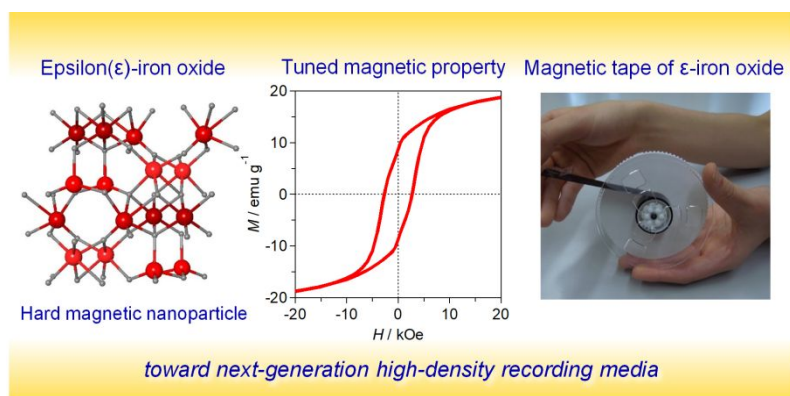
Advances in magnetic films of ϵ -iron oxide toward next-generation high-density recording media

Hiroko Tokoro,^{*,a,b} Asuka Namai^a and Shin-ichi Ohkoshi^{*,a}

^a Department of Materials Science, Faculty of Pure and Applied Sciences, University of Tsukuba, Tsukuba, Japan

^b Department of Chemistry, School of Science, The University of Tokyo, Tokyo, Japan

Table of contents entry



Recent developments in magnetic films composed of epsilon-iron oxide are introduced.

The film performance is studied and improved toward the next-generation of high-density magnetic recording media.

ARTICLE

Advances in magnetic films of epsilon-iron oxide toward next-generation high-density recording media

Hiroko Tokoro,^{*a,b} Asuka Namai^a and Shin-ichi Ohkoshi^{*a}Received 00th January 20xx,
Accepted 00th January 20xx

DOI: 10.1039/x0xx00000x

Iron oxide magnets, which are composed of the common elements iron and oxygen, are called ferrite magnets. They have diverse applications because they are chemically stable and inexpensive. Epsilon-iron oxide (ϵ -Fe₂O₃) is a polymorph that shows an extremely large coercive field as a magnetic oxide. It maintains its ferromagnetic ordering even when downsized to a single nano-sized scale (i.e., < 10 nm). Due to these characteristics, ϵ -Fe₂O₃ is highly expected to be used for high-density magnetic recording media in the big data era. Here, we describe the recent developments of magnetic films composed of metal-substituted ϵ -iron oxide, ϵ -M_xFe_{2-x}O₃ (*M*: substitution metal), toward the next-generation of magnetic media.

1. Introduction

The big-data era requires high-density magnetic recording media with a long-term guarantee.¹⁻⁵ Next-generation magnetic recording tapes should meet these requirements. Current magnetic recording tapes, which are typically composed of spindle-shaped cobalt-iron alloy nanoparticles or barium ferrite nanoparticles, provide long-term storage to archive data in diverse fields, including insurance, finance, broadcasting, and web services. However, magnetic materials used in magnetic tapes must be downsized to realize high-density media.⁶⁻¹⁰ This will not simply be achieved by downsizing the magnetic filler for two reasons. First, its pyrophoric character makes downsizing a challenge. Second, its magnetic ordering disappears upon downsizing.

On the other hand, epsilon-iron oxide (ϵ -Fe₂O₃) holds promise as next-generation high-density magnetic recording media as it has a large coercive field (H_c) over 20 kOe at room temperature. A single phase of ϵ -Fe₂O₃ was first synthesized in 2004,¹¹ and since then, it has been investigated in both basic and applied research.¹²⁻³⁴ The ferromagnetic property of ϵ -Fe₂O₃ is observed even upon downsizing to a single nanometre scale, indicating that its superparamagnetic limit (d_s) is very small ($d_s \sim 7.5$ nm), which is smaller than that of other ferrites (Fig. S1).³⁵

Herein we report the recent advances in ϵ -iron oxide magnetic films. First, we describe rhodium (Rh) substitution on a part of the Fe site of ϵ -iron oxide, ϵ -Rh_{0.14}Fe_{1.86}O₃, which realizes a huge H_c magnetic film (45 kOe).³⁶ Second, we introduce the angular dependence of the magnetic film using a highly oriented film of gallium (Ga) substituted ϵ -iron oxide, ϵ -Ga_{0.45}Fe_{1.55}O₃.³⁷ Third, we demonstrate magnetic recording on a magnetic tape of trimetal-

substituted ϵ -iron oxide, ϵ -Ga_{0.31}Ti_{0.05}Co_{0.05}Fe_{1.59}O₃, as a first step toward the application of ϵ -iron oxide as high-density magnetic recording media.³⁸

2. Large coercive field observed in a magnetic film on Rh-substituted epsilon-iron oxide

Although there are various important parameters such as the energy product in the magnetic properties, the coercive field H_c is a significant parameter. Magnetic ferrite is an insulator magnet with a relatively small H_c value, compared with a hard magnetic metal.³⁹⁻⁴³ In general, increasing the H_c value in magnetic ferrites is a challenging issue. However, ϵ -iron oxide (ϵ -Fe₂O₃) and metal substituted ϵ -iron oxides (ϵ -M_xFe_{2-x}O₃; *M* = substitution metal ions), exhibit large H_c values at room temperature and hold promise for magnetic media.⁴⁴⁻⁵⁰ In this section, we show a crystallographically oriented Rh-substituted ϵ -iron oxide nanoparticle-based magnetic film. It exhibits the largest H_c values for magnetic ferrites reported to date, 45 kOe at 200 K and 35 kOe at 300 K.

The magnetic film based on Rh-substituted ϵ -Fe₂O₃, ϵ -Rh_{0.14}Fe_{1.86}O₃, was obtained as follows. An impregnation method, which involved mesoporous silica nanoparticles as a template,²¹ was used to synthesize rhodium-substituted ϵ -iron oxide nanoparticles as an inorganic filler. The rhodium-substituted ϵ -iron oxide nanoparticles were subsequently mixed with a urethane resin and a vinyl chloride polymer in an applied external magnetic field to produce an oriented magnetic film (Fig. 1). The direction of the applied magnetic field is the out-of-plane direction of the film (*z*-axis). Figure 2 illustrates that it has an orthorhombic structure in the *Pna*2₁ space group.

To examine the degree of orientation of the nanocrystals inside the obtained film, we measured the X-ray diffraction (XRD) pattern. Figure 3a shows the XRD pattern for a powder sample, while Figure 3b shows that of an oriented film. A strong peak appears at 35.2° due to the 200 reflection. Next, the relationship between the XRD peak

^a Department of Chemistry, School of Science, The University of Tokyo, 7-3-1 Hongo, Bunkyo-ku, Tokyo 113-0033, Japan
E-mail: Ohkoshi@chem.s.u-tokyo.ac.jp

^b Department of Materials Science, Faculty of Pure and Applied Sciences, University of Tsukuba, 1-1-1 Tennodai, Tsukuba, Ibaraki 305-8573, Japan
E-mail: tokoro@ims.tsukuba.ac.jp

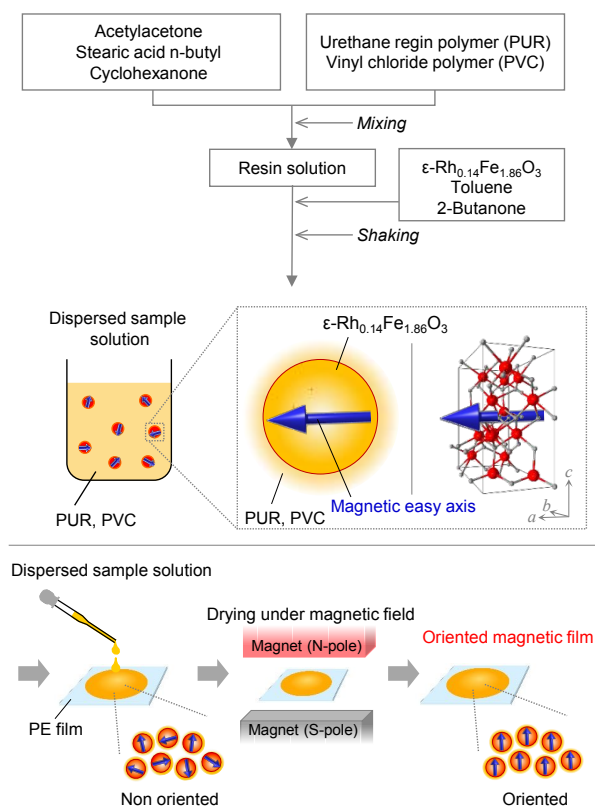


Figure 1. Flowchart of the synthesis of a crystallographically oriented thin film of ϵ - $\text{Rh}_{0.14}\text{Fe}_{1.86}\text{O}_3$: Preparation of the vehicle resin solution, addition of the ϵ - $\text{Rh}_{0.14}\text{Fe}_{1.86}\text{O}_3$ powder sample, preparation of a dispersed sample solution by mixing and shaking with zirconia balls, and preparation of an oriented magnetic film by casting the dispersed sample solution on a polyester (PE) film and drying under a magnetic field. Blue arrows represent the spontaneous magnetization of the ϵ - $\text{Rh}_{0.14}\text{Fe}_{1.86}\text{O}_3$ nanoparticles, which are represented as orange balls. The middle figure shows the crystal structure of ϵ - $\text{Rh}_{0.14}\text{Fe}_{1.86}\text{O}_3$ nanoparticle where red and gray balls represent the Fe and O atoms, respectively. Adapted with permission from J. Am. Chem. Soc., 2017, 139, 13268–13271. ©2017 American Chemical Society.

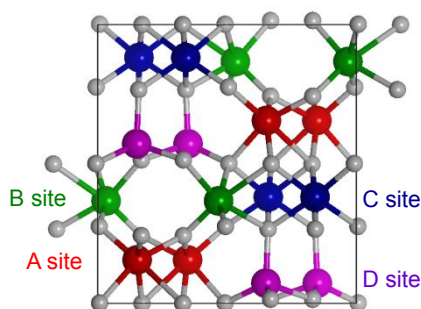


Figure 2. Schematic representation of the ϵ - Fe_2O_3 crystal structure shown from the a -axis direction. Red, green, and blue balls represent the Fe ions at the octahedral A, B, and C sites, respectively. Magenta balls represent Fe ions at the tetrahedral D sites. Grey balls represent the oxygen ions. Adapted with permission from J. Am. Chem. Soc., 2017, 139, 13268–13271. ©2017 American Chemical Society.

intensities of the oriented sample (I_{orient}) and those of the non-oriented sample ($I_{\text{nonorient}}$) was used to determine the degree of orientation. The Lotgering factor f ($0 \leq f \leq 1$) indicates the degree of orientation. It is expressed as $f = (P_{\text{orient}} - P_{\text{nonorient}}) / (1 - P_{\text{nonorient}})$, where P_{orient} and $P_{\text{nonorient}}$ are the area ratios of the 200 reflection for

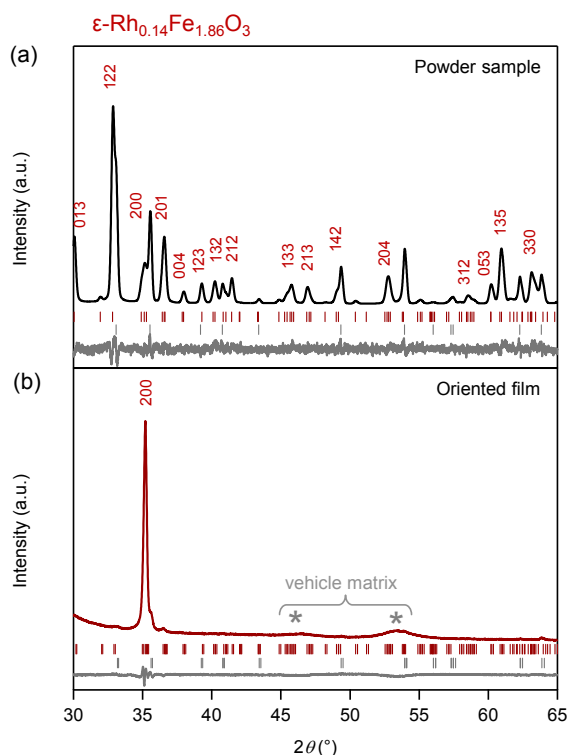


Figure 3. XRD patterns and Rietveld analyses of rhodium substituted ϵ -iron oxide (a) in the powder-form and (b) as an oriented film. Asterisks represent the peaks from vehicle matrix. Adapted with permission from J. Am. Chem. Soc., 2017, 139, 13268–13271. © 2017 American Chemical Society.

oriented and non-oriented nanocrystals, respectively (*i.e.*, $P = I_{200} / \sum I_{hkl}$). The film exhibits a remarkably high f value of 0.96. Hence, its crystallographic a -axis is almost perfectly oriented perpendicular to the film.

The magnetic hysteresis loops of the prepared film at 300 K was measured. During the hysteresis measurement in the superconducting quantum interference device magnetometer, the external magnetic field (H_{ex}) is applied to the film in the perpendicular ($H_{\text{ex}} \perp z$ -axis) and parallel directions ($H_{\text{ex}} // z$ -axis). The H_c value reaches 35 kOe when $H_{\text{ex}} // z$ -axis (Fig. 4a). Such a huge H_c value is attributed to two factors: (i) the orbital angular momentum of the distorted octahedral iron sites (A and B sites) generated by the strong iron-oxygen hybridization and (ii) the orbital angular momentum contribution of the rhodium ion.⁴⁵ The magnetization value at $H_{\text{ex}} = 70$ kOe (M_s) is 9.5 emu g^{-1} , while the remnant magnetization (M_r) is 7.9 emu g^{-1} (for unsubstituted ϵ - Fe_2O_3 , the M_s and M_r values are 16.1 emu g^{-1} and 12.3 emu g^{-1} , respectively).²⁹ On the other hand, the magnetic hysteresis loop where $H_{\text{ex}} \perp z$ -axis exhibits much smaller values. That is, the H_c value is 5 kOe, while the M_r value is 1.4 emu g^{-1} .

Furthermore, we measured the temperature dependence of the magnetic hysteresis loop. As the temperature decreases from 300 K, the magnetic hysteresis loop becomes larger (Fig. 4b). H_c reaches a maximum value 45 kOe at 200 K. It decreases sigmoidally, which is centered at 120 K, and reaches a value of 7.1 kOe at 10 K. A similar temperature dependence of H_c has been reported in a series of ϵ - Fe_2O_3 and ϵ - $M_x\text{Fe}_{2-x}\text{O}_3$.^{51–55} For example, ϵ - $\text{In}_{0.24}\text{Fe}_{1.76}\text{O}_3$ undergoes a phase transition from ferrimagnetism to antiferromagnetism at 200 K.⁵⁵ This behaviour is well investigated (e.g., by synchrotron x-ray

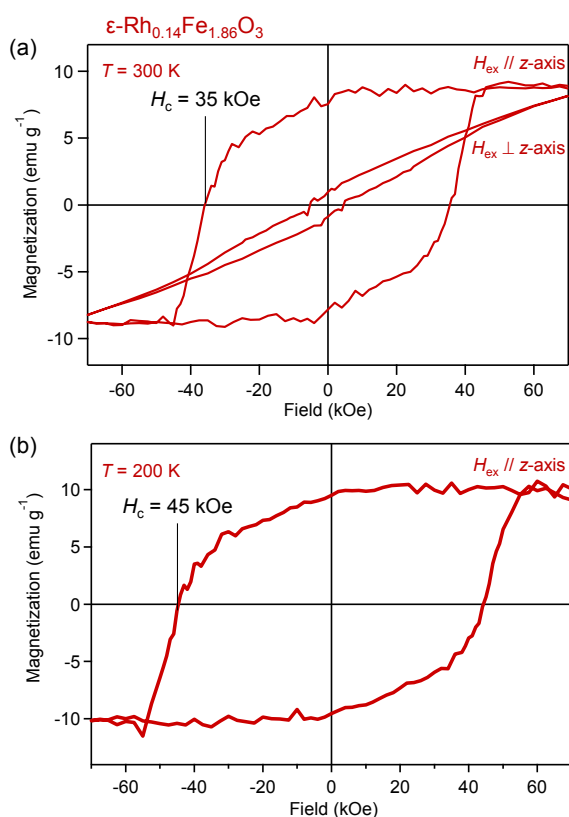


Figure 4. (a) Magnetization versus external magnetic field plots of $\epsilon\text{-Rh}_{0.14}\text{Fe}_{1.86}\text{O}_3$ at 300 K. External parallel magnetic field (closed circles) and external perpendicular magnetic field (open circles) to the z -axis direction were used for measurements. (b) Magnetization versus external magnetic field plots of $\epsilon\text{-Rh}_{0.14}\text{Fe}_{1.86}\text{O}_3$ at 200 K. Adapted with permission from J. Am. Chem. Soc., 2017, 139, 13268–13271. © 2017 American Chemical Society.

Powder diffraction (SXRPD), neutron powder diffraction, Mössbauer spectroscopy, heat capacity, x-ray magnetic circular dichroism, and magnetic measurements). The origins are suggested as changes of the exchange interaction and magnetic anisotropy arising from a structural transformation.^{56,57}

Summarizing above, we obtained a crystallographically oriented Rh-substituted ϵ -iron oxide, $\epsilon\text{-Rh}_{0.14}\text{Fe}_{1.86}\text{O}_3$, that is an almost perfectly oriented magnetic thin film (*i.e.*, a Lotgering factor of 0.96). The film exhibits remarkably large coercive fields with the largest H_c values among magnetic ferrites of 45 kOe at 200 K and 35 kOe at 300 K.

3. Angular dependence of the magnetic hysteresis loops of a magnetic film composed of Ga-substituted epsilon-iron oxide

In 2004, $\epsilon\text{-Fe}_2\text{O}_3$ was first reported as a hard-magnetic ferrite.¹¹ It has great potential as a next-generation recording material. Crystallographically oriented ϵ -iron oxide magnetic films allow the angular dependence of the magnetic properties of nanomagnetic particles to be investigated. In this section, we discuss the angular dependence of the magnetic hysteresis loops for a crystallographically oriented $\epsilon\text{-Ga}_{0.45}\text{Fe}_{1.55}\text{O}_3$ magnetic film.

$\epsilon\text{-Ga}_{0.45}\text{Fe}_{1.55}\text{O}_3$, a nanomagnetic material, was prepared according to the literature.⁵⁸ The nanoparticles are 25 ± 11 nm spheres. The powder sample displays an orthorhombic structure in the $Pna2_1$ space group, where Ga selectively substitutes for the D site. Figure 5a confirms a magnetic hysteresis loop of $\epsilon\text{-Ga}_{0.45}\text{Fe}_{1.55}\text{O}_3$ with a large H_c value of 7.9 kOe and a magnetization value of 30.4 emu g^{-1} at 7 tesla (T) (M_{7T}) at 200 K. Then, we prepared a crystallographically oriented $\epsilon\text{-Ga}_{0.45}\text{Fe}_{1.55}\text{O}_3$ film using a dispersed resin solution composed of a urethane resin and a vinyl chloride polymer according to the previous section.³⁶

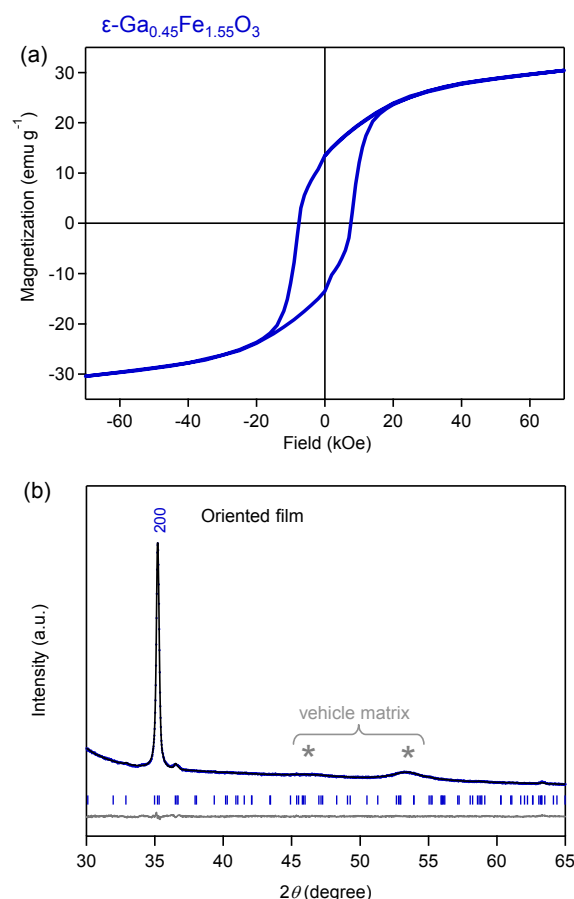


Figure 5. (a) Magnetization vs. external magnetic field curve of the $\epsilon\text{-Ga}_{0.45}\text{Fe}_{1.55}\text{O}_3$ powder form. (b) XRD pattern and Rietveld analyses of the $\epsilon\text{-Ga}_{0.45}\text{Fe}_{1.55}\text{O}_3$ film oriented in a magnetic field. Asterisks represent the peaks from the vehicle matrix. Adapted with permission from Eur. J. Inorg. Chem., 2018, 847–851. © 2018 WILEY - VCH Verlag GmbH & Co. KGaA, Weinheim.

The $\epsilon\text{-Ga}_{0.45}\text{Fe}_{1.55}\text{O}_3$ film displays a strong peak in the XRD pattern due to the 200 reflection (Fig. 5b). It has a high f factor of 0.94. Figure 6a plots the angular dependence of the magnetic hysteresis loops when the angle (θ) is set to 0° , 15° , 30° , 45° , 60° , 75° , or 90° . It should be noted that $\theta = 0^\circ$ indicates that the measured magnetic field is parallel to the out-of-plane direction of the film. The H_c values are 9.7 kOe ($\theta = 0^\circ$), 8.4 kOe ($\theta = 15^\circ$), 7.5 kOe ($\theta = 30^\circ$), 7.0 kOe ($\theta = 45^\circ$), 6.7 kOe ($\theta = 60^\circ$), 5.5 kOe ($\theta = 75^\circ$), and 4.3 kOe ($\theta = 90^\circ$). The M_{7T} values are 30.4 emu g^{-1} ($\theta = 0^\circ$) and 28.8 emu g^{-1} ($\theta = 90^\circ$). Additionally, we calculated the magnetic hysteresis loops for various θ angles, considering the f factor is 0.94. Figure 6b shows that the calculated and observed curves agree well.

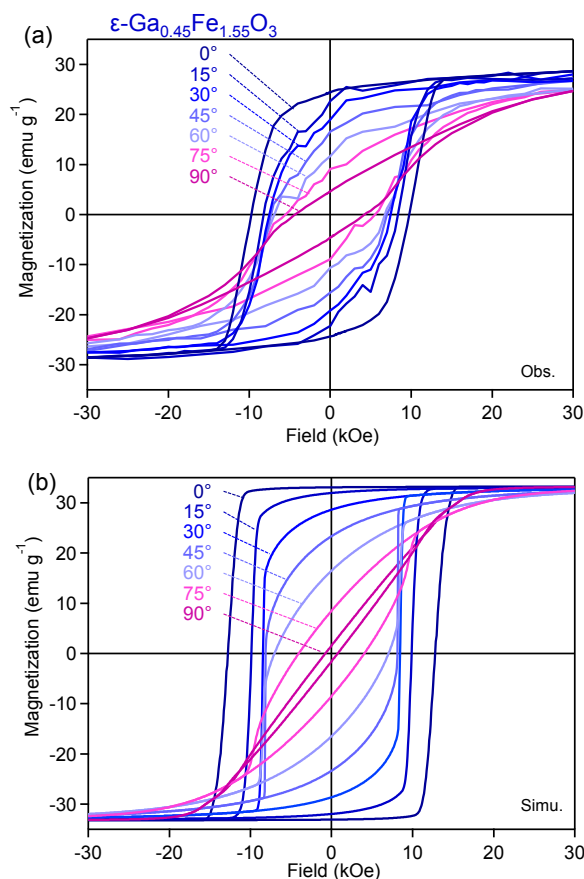


Figure 6. Angular dependence of the magnetic hysteresis loops. (a) Magnetization vs. external magnetic field curve of the $\epsilon\text{-Ga}_{0.45}\text{Fe}_{1.55}\text{O}_3$ magnetic film oriented crystallographically at 0° , 15° , 30° , 45° , 60° , 75° , and 90° . (b) Simulated magnetization (M) vs. external magnetic field (H) curve of the film oriented in a magnetic field at 0° , 15° , 30° , 45° , 60° , 75° , and 90° . Adapted with permission from Eur. J. Inorg. Chem., 2018, 847–851. © 2018 WILEY - VCH Verlag GmbH & Co. KGaA, Weinheim.

As above, we realized a magnetic film composed of crystallographically oriented $\epsilon\text{-Ga}_{0.45}\text{Fe}_{1.55}\text{O}_3$ nanoparticles in a vehicle resin where the crystallographic a -axis is aligned along the out-of-plane direction of the film. Then a rectangular magnetic hysteresis loop with an H_c value of 9.7 kOe and M_s value of 30.4 emu g^{-1} at room temperature is observed when $\theta = 0^\circ$.

4. Trimetal-substituted ϵ -iron oxide for next-generation magnetic recording media

Magnetic recording tapes are expected to play an important role in the big data era due to their long-term stability and low cost.^{1–4} ϵ -iron oxide, $\epsilon\text{-Fe}_2\text{O}_3$, exhibits a large H_c over 20 kOe at room temperature, and is a promising candidate for high-density magnetic recording media. The H_c of a magnetic nanomaterial is strongly related to its particle size. As the particle size decreases, H_c decreases due to the superparamagnetic effect (i.e., thermal excitation leads to magnetization inversion and a decreased coercive field (Fig. S1)). For high-density recording, smaller particle sizes of the magnetic material are important. However, H_c should be adjusted to 3 kOe for

practical applications as next-generation high-density storage media. ϵ -iron oxide can be substituted with multiple metals. Here, we focus on $\epsilon\text{-Ga}^{\text{III}}_{0.31}\text{Ti}^{\text{IV}}_{0.05}\text{Co}^{\text{II}}_{0.05}\text{Fe}^{\text{III}}_{1.59}\text{O}_3$, which is simultaneously substituted with Ga^{3+} , Ti^{4+} , and Co^{2+} ions.⁵⁹ It exhibits an H_c value of 2.7 kOe, suitable for a high-density magnetic memory. As a proof of concept, we prepared a practical $\epsilon\text{-Ga}^{\text{III}}_{0.31}\text{Ti}^{\text{IV}}_{0.05}\text{Co}^{\text{II}}_{0.05}\text{Fe}^{\text{III}}_{1.59}\text{O}_3$ magnetic recording tape and demonstrated its performance.

$\epsilon\text{-Ga}_{0.31}\text{Ti}_{0.05}\text{Co}_{0.05}\text{Fe}_{1.59}\text{O}_3$ was fabricated via the sol-gel method.⁵⁷ Figure 7 shows the sample has an isomorphic orthorhombic crystal structure with $\epsilon\text{-Fe}_2\text{O}_3$ in the $Pna2_1$ space group. It is composed of spherical nanoparticles with a particle size of $18.3 \pm 8.8 \text{ nm}$ (Fig. 7, inset). The D sites are mainly substituted with Ga^{3+} , Ti^{4+} , and Co^{2+} ions. Specifically, 48%, 10%, and 10% of the D sites are occupied by Ga^{3+} , Ti^{4+} , and Co^{2+} , respectively. In addition, 14% of the C sites are occupied by Ga^{3+} .

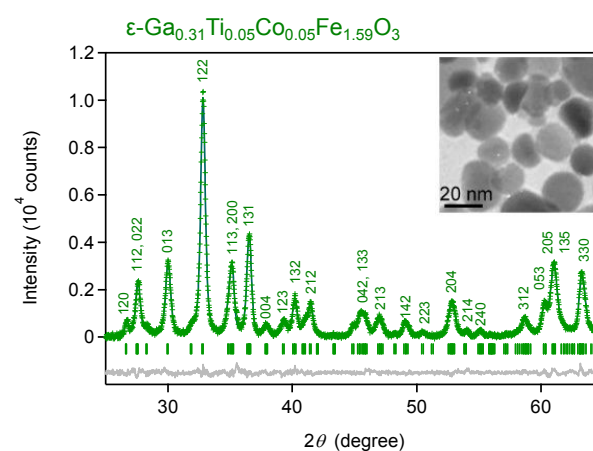


Figure 7. XRPD pattern and Rietveld analysis of $\epsilon\text{-Ga}_{0.31}\text{Ti}_{0.05}\text{Co}_{0.05}\text{Fe}_{1.59}\text{O}_3$. Green crosses, black line, and grey line are the observed pattern, calculated pattern, and their difference, respectively. Green bars represent the calculated positions of the Bragg reflections of the ϵ -phase (orthorhombic, $Pna2_1$). Inset is the TEM image. Adapted with permission from Angew. Chem. Int. Ed., 2016, 55, 11403–11406 © 2016 WILEY - VCH Verlag GmbH & Co. KGaA, Weinheim.

Figure 8 plots the magnetization versus magnetic field curve at 300 K. Compared to the original $\epsilon\text{-Fe}_2\text{O}_3$, which has a magnetization value of 16.2 emu g^{-1} at 7 T, $\epsilon\text{-Ga}_{0.31}\text{Ti}_{0.05}\text{Co}_{0.05}\text{Fe}_{1.59}\text{O}_3$ has a 44% increase in the magnetization value (23.4 emu g^{-1}) due to the reduced sublattice magnetization at the D sites because Fe^{3+} ions ($S = 5/2$) are substituted with Ga^{3+} ($S = 0$), Ti^{4+} ($S = 0$), and Co^{2+} ($S = 3/2$). Moreover, the H_c value of $\epsilon\text{-Ga}_{0.31}\text{Ti}_{0.05}\text{Co}_{0.05}\text{Fe}_{1.59}\text{O}_3$ is 2.7 kOe. This is one order smaller than the H_c value of the original $\epsilon\text{-Fe}_2\text{O}_3$. The smaller H_c value is attributed to the compensation of single-ion anisotropies of Fe^{3+} and the additional Co^{2+} . As the H_c value is suitable for magnetic recordings ($<3 \text{ kOe}$), we investigated its feasibility as magnetic recording media.

Figure 9a shows a photograph of the trial magnetic tape. Figure 9b shows a cross section scanning electron microscopy (SEM) image of the manufactured magnetic tape. The magnetic layer has a thickness of $110 \pm 5 \text{ nm}$ and a very low surface roughness of 2.7 nm. The nanoparticles are crystallographically oriented.

We evaluated its performance using a third-generation linear tape-open (LTO-3) anisotropic magnetoresistive (AMR) head. Figure

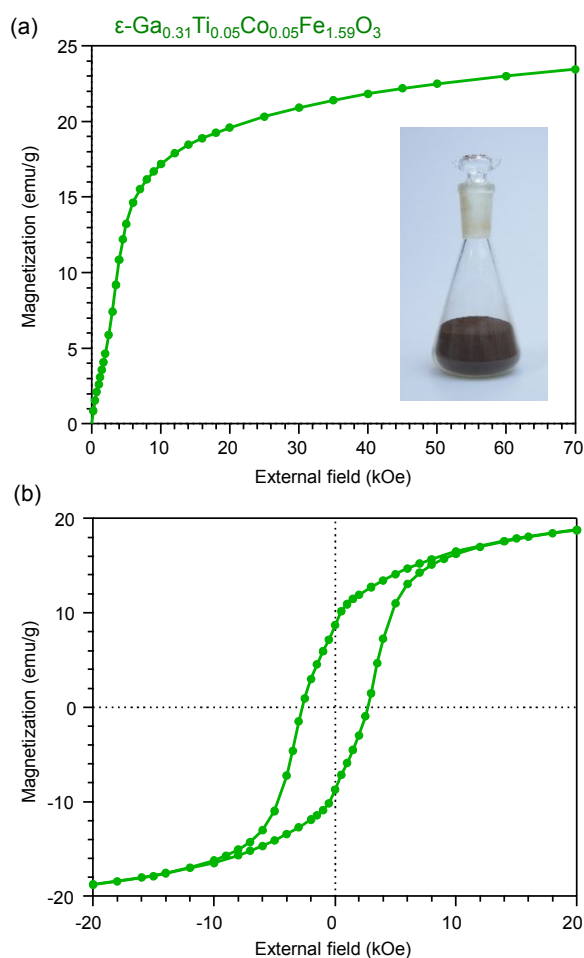


Figure 8. (a) Initial magnetization curve and (b) magnetic hysteresis loop of $\epsilon\text{-Ga}_{0.31}\text{Ti}_{0.05}\text{Co}_{0.05}\text{Fe}_{1.59}\text{O}_3$ measured at 300 K. Inset of (a) is a photograph of the powder sample. Adapted with permission from *Angew. Chem. Int. Ed.*, 2016, 55, 11403–11406 © 2016 WILEY - VCH Verlag GmbH & Co. KGaA, Weinheim.

9c compares the results to those of a cobalt-iron metal alloy (MP1, DOWA Electronics Materials) magnetic tape. Compared to the MP1 magnetic tape, the peak of the $\epsilon\text{-Ga}_{0.31}\text{Ti}_{0.05}\text{Co}_{0.05}\text{Fe}_{1.59}\text{O}_3$ tape is sharper, the foot is much narrower, and the baseline is perfectly flat, demonstrating that the $\epsilon\text{-Ga}_{0.31}\text{Ti}_{0.05}\text{Co}_{0.05}\text{Fe}_{1.59}\text{O}_3$ magnetic tape has a high signal-to-noise ratio (S/N). Consequently, $\epsilon\text{-Ga}_{0.31}\text{Ti}_{0.05}\text{Co}_{0.05}\text{Fe}_{1.59}\text{O}_3$ holds promise in next-generation magnetic tape-recording applications.

As above, we developed $\epsilon\text{-Ga}^{\text{III}}_{0.31}\text{Ti}^{\text{IV}}_{0.05}\text{Co}^{\text{II}}_{0.05}\text{Fe}^{\text{III}}_{1.59}\text{O}_3$. It has an average size of 18 nm. More importantly, the magnetic properties of ϵ -iron oxide can be tuned by adjusting the substitution ratios of the Ga^{3+} , Ti^{4+} , and Co^{2+} cations. Hence, $\epsilon\text{-Ga}^{\text{III}}_{0.31}\text{Ti}^{\text{IV}}_{0.05}\text{Co}^{\text{II}}_{0.05}\text{Fe}^{\text{III}}_{1.59}\text{O}_3$ has potential as practical and economical magnetic recording media that can be tuned to different specifications for data storage in the big data era.

Conclusions

It has been sixteen years since $\epsilon\text{-Fe}_2\text{O}_3$ was firstly reported as a hard-magnetic ferrite with a large coercive field. To date, basic studies have elucidated its physical properties. In addition, research towards practical applications has made great strides.

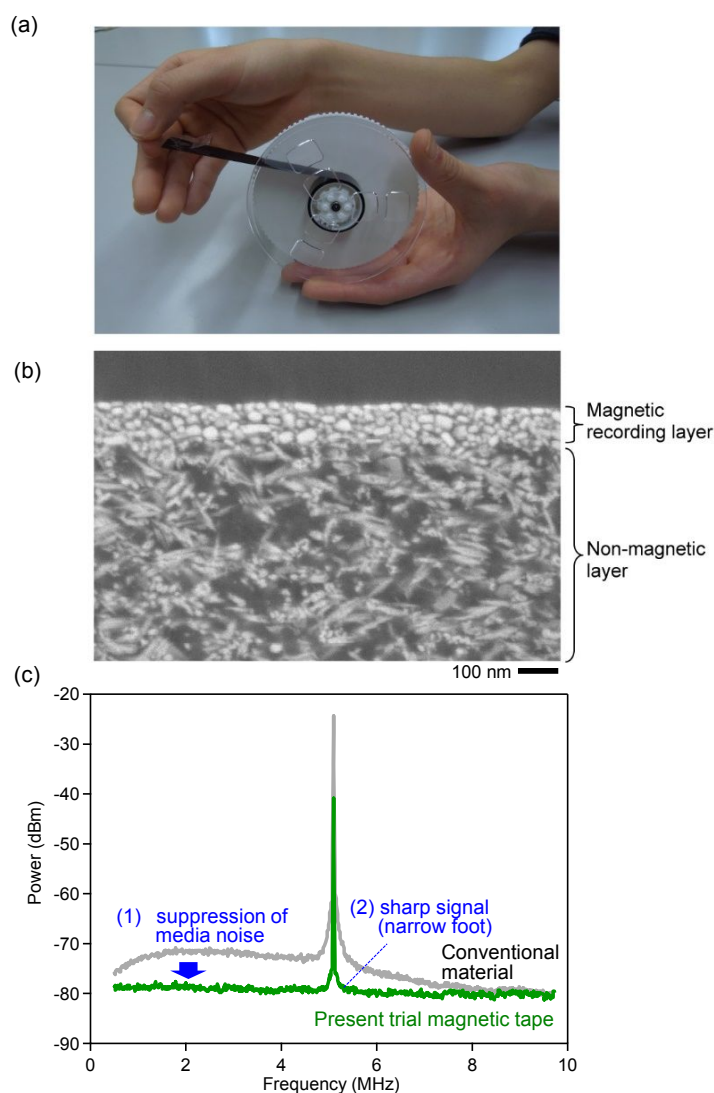


Figure 9. (a) Image of the manufactured $\epsilon\text{-Ga}_{0.31}\text{Ti}_{0.05}\text{Co}_{0.05}\text{Fe}_{1.59}\text{O}_3$ magnetic recording tape. (b) Cross-sectional SEM image of the $\epsilon\text{-Ga}_{0.31}\text{Ti}_{0.05}\text{Co}_{0.05}\text{Fe}_{1.59}\text{O}_3$ magnetic recording tape and cobalt-iron alloy tape signal measured with the LTO-3 AMR head. Adapted with permission from *Angew. Chem. Int. Ed.*, 2016, 55, 11403–11406 © 2016 WILEY - VCH Verlag GmbH & Co. KGaA, Weinheim.

Data storage is classified into three categories depending on the access frequency; hot data, warm data, and cold data. Especially, for cold data, magnetic recording tapes are expected to play an important role in the big data era due to their long-term stability and low cost.^{1–5} In the present article, we described a ϵ -iron oxide magnetic film developed as a next-generation high-density magnetic recording material.

In addition to magnetic recording materials, ϵ -iron oxide could have various practical applications, e.g., a probe-lever for magnetic force microscopy (MFM),²⁹ magnetic hyperthermia nanoparticles for medical use,³⁴ and millimeter-wave absorption materials.^{44,45,50,58}

Conflicts of interest

There are no conflicts to declare.

Acknowledgements

The present research was supported in part by JSPS KAKENHI (Grant Number 16H06521), Coordination Asymmetry, Scientific Research (A) (Grant Number 20H00369), JSPS Grant-in-Aid for specially promoted Research (Grant Number 15H05697), Grant for Young Researchers (18K13989), A-STEP from JST, DOWA Technofond, and MEXT Q-LEAP (JPMXS 0118068681). We also acknowledge the Cryogenic Research Center, The University of Tokyo, and Nanotechnology Platform, which are supported by MEXT. We are grateful to Ms. M. Yoshikiyo and Dr. K. Imoto for technical support.

Notes and references

- G. Cherubini, C. C. Chung, W. C. Messner and S. O. R. Moheimani, *IEEE Trans. Contr. Syst. Tech.*, 2012, **20**, 296–322.
- H. Nishio and H. Yamamoto, *IEEE Trans. Magn.*, 2010, **46**, 3747–3751.
- R. E. Fontana Jr., G. M. Decad and S. R. Hetzler, *J. Appl. Phys.*, 2015, **117**, 17E301.
- S. Ohkoshi, K. Imoto, A. Namai, M. Yoshikiyo, S. Miyashita, H. Qiu, S. Kimoto, K. Kato and M. Nakajima, *J. Am. Chem. Soc.*, 2019, **141**, 1775–1780.
- S. Ohkoshi, M. Yoshikiyo, K. Imoto, K. Nakagawa, A. Namai, H. Tokoro, K. Takeuchi, F. Jia, S. Miyashita, M. Nakajima, H. Qiu, K. Kato, T. Yamaoka, M. Shirata, K. Naoi, K. Yagishita, and H. Doshita, *Adv. Mater.*, 2004897 (2020).
- M. L. Plumer, J. van Ek and D. Weller, *The Physics of Ultra-High Density Magnetic Recording*, Springer, Berlin, 2001.
- W. A. Challener, C. Peng, A. V. Itagi, D. Karns, W. Peng, Y. Peng, X. M. Yang, X. Zhu, N. J. Gokemeijer, Y.-T. Hsia, G. Ju, R. E. Rottmayer, M. A. Seigler and E. C. Gage, *Nature Photon.*, 2009, **3**, 220–224.
- T. Hayashi, S. Hirono, M. Tomita and S. Umemura, *Nature*, 1996, **381**, 772–774.
- I. Tudosa, C. Stamm, A. B. Kashuba, F. King, H. C. Siegmann, J. Stöhr, G. Ju, B. Lu and D. Weller, *Nature*, 2004, **428**, 831–833.
- D. Alloyeau, C. Ricolleau, C. Mottet, T. Oikawa, C. Langlois, Y. Le Bouar, N. Braidy and A. Loiseau, *Nature Mater.*, 2009, **8**, 940–946.
- J. Jin, S. Ohkoshi and K. Hashimoto, *Adv. Mater.*, 2004, **16**, 48–51.
- S. Ohkoshi and H. Tokoro, *Bull. Chem. Soc. Jpn.*, 2013, **86**, 897–907.
- E. Tronc, C. Chaneac, J. P. Jolivet and J. M. Greneche, *J. Appl. Phys.*, 2005, **98**, 053901/1–4.
- J. Jin, K. Hashimoto and S. Ohkoshi, *J. Mater. Chem.*, 2005, **15**, 1067–1071.
- K. Kelm and W. Mader, *Z. Anorg. Allg. Chem.*, 2005, **631**, 2383–2389.
- Y. Kusano, T. Fujii, J. Takada, M. Fukuhara, A. Doi, Y. Ikeda and M. Takano, *Chem. Mater.*, 2008, **20**, 151–156.
- S. Sakurai, K. Tomita, K. Hashimoto, H. Yashiro and S. Ohkoshi, *J. Phys. Chem. C*, 2008, **112**, 20212–20216.
- Y. Ding, J. R. Morber, R. L. Snyder and Z. L. Wang, *Adv. Funct. Mater.*, 2007, **17**, 1172–1178.
- E. Taboada, M. Gich and A. Roig, *ACS Nano*, 2009, **3**, 3377–3382.
- P. Brázda, D. Nižňanský, J.-L. Rehspringer and J.P. Vejpravová, *J. Sol-Gel Sci. Technol.*, 2009, **51**, 78–83.
- S. Sakurai, A. Namai, K. Hashimoto and S. Ohkoshi, *J. Am. Chem. Soc.*, 2009, **131**, 18299–18303.
- J. Tuček, S. Ohkoshi and R. Zbořil, *Appl. Phys. Lett.*, 2011, **99**, 253108/1–3.
- C. Stötzl, H.D. Kurland, J. Grabow, S. Dutz, E. Müller, M. Sierka and F. A. Müller, *Cryst. Growth Des.*, 2013, **13**, 4868–4876.
- G. Carraro, C. Maccato, A. Gasparotto, T. Montini, S. Turner, O. I. Lebedev, V. Gombac, G. Adami, G.V. Tendeloo, D. Barreca and P. Fornasiero, *Adv. Funct. Mater.*, 2014, **24**, 372–378.
- M. Gich, I. Fina, A. Morelli, F. Sánchez, M. Alexe, J. Gàzquez, J. Fontcuberta and A. Roig, *Adv. Mater.*, 2014, **26**, 4645–4652.
- D. A. Balaev, I. S. Poperechny, A. A. Krasikov, K. A. Shaikhutdinov, A. A. Dubrovskiy, S. I. Popkov, A. D. Balaev, S. S. Yakushkin, G. A. Bukhtiyarova, O. N. Martyanov and Y. L. Raikher, *J. Appl. Phys.*, 2015, **117**, 063908/1–6.
- A. Erlebach, H.-D. Kurland, J. Grabow, F. Müller and M. Sierka, *Nanoscale*, 2015, **7**, 2960–2969.
- J. López-Sánchez, A. Serrano, A. D. Campo, M. Abuín, O. R. Fuente and N. Carmona, *Chem. Mater.*, 2016, **28**, 511–518.
- S. Ohkoshi, A. Namai, T. Yamaoka, M. Yoshikiyo, K. Imoto, T. Nasu, S. Anan, Y. Umeta, K. Nakagawa and H. Tokoro, *Sci. Rep.*, 2016, **6**, 27212/1–10.
- J. L. García-Muñoz, A. Romaguera, F. Fauth, J. Nogués and M. Gich, *Chem. Mater.*, 2017, **29**, 9705–9713.
- K. Knizek, M. Pashchenko, P. Levinsky, O. Kaman, J. Houdkova, P. Jiricek, J. Hejtmanek, M. Soroka and J. Bursik, *J. Appl. Phys.*, 2018, **124**, 21/1–6.
- H. Tokoro, W. Tarora, A. Namai, M. Yoshikiyo and S. Ohkoshi, *Chem. Mater.*, 2018, **30**, 2888–2894.
- J. A. Sans, V. Monteseguro, G. Garbarino, M. Gich, V. Cerantola, V. Cuartero, M. Monte, T. Irifune, A. Muñoz and C. Popescu, *Nat. Commun.*, 2018, **9**, 4554/1–11.
- Y. Gu, M. Yoshikiyo, A. Namai, D. Bonvin, A. Martinez, R. Piñol, P. Téllez, N. J. O. Silva, F. Ahrentorp, C. Johansson, J. Marco-Brualla, R. Moreno-Loshuertos, P. Fernández-Silva, Y. Cui, S. Ohkoshi and A. Millán, *RSC Adv.*, 2020, **10**, 28786–28797.
- S. Ohkoshi, A. Namai, K. Imoto, M. Yoshikiyo, W. Tarora, K. Nakagawa, M. Komine, Y. Miyamoto, T. Nasu, S. Oka and H. Tokoro, *Sci. Rep.*, 2015, **5**, 14414/1–9.
- S. Ohkoshi, K. Imoto, A. Namai, S. Anan, M. Yoshikiyo and H. Tokoro, *J. Am. Chem. Soc.*, 2017, **139**, 13268–13271.
- M. Yoshikiyo, A. Namai, K. Imoto, S. Anan, H. Tokoro and S. Ohkoshi, *Eur. J. Inorg. Chem.*, 2018, 847–851.
- S. Ohkoshi, A. Namai, M. Yoshikiyo, K. Imoto, K. Tamasaki, K. Matsuno, O. Inoue, T. Ide, K. Masada, M. Goto, T. Goto, T. Yoshida and T. Miyazaki, *Angew. Chem. Int. Ed.*, 2016, **55**, 11403–11406.
- K. H. J. Buschow, *Handbook of Magnetic Materials*, Elsevier, Amsterdam, 1995.
- R. M. Cornell and U. Schwertmann, *The Iron Oxide: Structure, Properties, Reactions, Occurrences and Uses.*, Wiley-VCH, Weinheim, 2003.
- B. D. Cullity and C. D. Graham, *Introduction to Magnetic Materials*, Wiley-IEEE Press, Hoboken, 2008.
- J. M. D. Coey, *Magnetism and Magnetic Materials*, Cambridge University Press, Cambridge, 2010.
- R.C. Pullar, *Prog. Mater. Sci.*, 2012, **57**, 1191–1334.
- A. Namai, S. Sakurai, M. Nakajima, T. Suemoto, K. Matsumoto, M. Goto, S. Sasaki and S. Ohkoshi, *J. Am. Chem. Soc.*, 2009, **131**, 1170–1173.
- A. Namai, M. Yoshikiyo, K. Yamada, S. Sakurai, T. Goto, T. Yoshida, T. Miyazaki, M. Nakajima, T. Suemoto, H. Tokoro and S. Ohkoshi, *Nat. Commun.*, 2012, **3**, 1035/1–6.
- T. Katayama, S. Yasui, Y. Hamasaki and M. Itoh, *Appl. Phys. Lett.*, 2017, **110**, 212905.

- 47 L. Corbellini, C. Lacroix, D. Ménard and A. Pignolet, *Scr. Mater.*, 2017, **140**, 63–66.
- 48 A. Namai and S. Ohkoshi, *Chem. Eur. J.*, 2018, **24**, 11880–11884.
- 49 T. Katayama, S. Yasui, T. Osakabe, Y. Hamasaki and M. Itoh, *Chem. Mater.*, 2018, **30**, 1436–1441.
- 50 A. Namai, K. Ogata, M. Yoshikiyo and S. Ohkoshi, *Bull. Chem. Soc. Jpn.*, 2020, **93**, 20–25.
- 51 M. Popovici, M. Gich, D. Niznansky, A. Roig, C. Savii, L. Casas, E. Molins, K. Zaveta, C. Enache, J. Sort, S. Brion, G. Chouteau and J. Nogués, *Chem. Mater.*, 2004, **16**, 5542–5548.
- 52 S. Sakurai, J. Jin, K. Hashimoto and S. Ohkoshi, *J. Phys. Soc. Jpn.*, 2005, **74**, 1946–1949.
- 53 M. Kurmoo, J. L. Rehspringer, A. Hutlova, C. D'Orléans, S. Vilminot, C. Estournès and D. Niznansky, *Chem. Mater.*, 2005, **17**, 1106–1114.
- 54 R. Jones, R. Nickel, P. K. Manna, J. Hilman and J. van Lierop, *Phys. Rev. B*, 2019, **100**, 094425/1–10.
- 55 S. Sakurai, S. Kuroki, H. Tokoro, K. Hashimoto and S. Ohkoshi, *Adv. Funct. Mater.*, 2007, **17**, 2278–2282.
- 56 M. Gich, C. Frontera, A. Roig, E. Taboada, E. Molins, H. R. Rechenberg, J. D. Ardisson, W. A. A. Macedo, C. Ritter, V. Hardy, J. Sort, V. Skumryev and J. Nogués, *Chem. Mater.*, 2006, **18**, 3889–3897.
- 57 Y. -C. Tseng, N. M. Souza-Neto, D. Haskel, M. Gich, C. Frontera, A. Roig, M. Veenendaal and J. Nogués, *Phys. Rev. B*, 2009, **79**, 094404/1–6.
- 58 S. Ohkoshi, S. Kuroki, S. Sakurai, K. Matsumoto, K. Sato and S. Sasaki, *Angew. Chem. Int. Ed.*, 2007, **46**, 8392–8395.
- 59 We selected Ga, Co, and Ti as the substitution metals. Ga is an important substituent metal that decreases the H_c and increases the magnetization. Co decreases the H_c more effectively than Ga. Since the valence states of Fe and Ga are trivalent but Co is divalent, tetravalent Ti was substituted to maintain a neutral charge balance.